CMS Physics Analysis Summary

Contact: cms-pag-conveners-exotica@cern.ch 2012/03/04

Search for the pair production of a fourth-generation up-type t′ quark in events with a lepton and at least four jets

The CMS Collaboration

Abstract

A search is presented for the pair production of a fourth-generation up-type t′ quark in proton-proton collisions at $\sqrt{s} = 7$ TeV using data collected by the Compact Muon Solenoid (CMS) experiment. The t′ quark is assumed to decay exclusively to a W boson and a b quark. The search is carried out using events with a single isolated electron or muon, large missing transverse momentum, and at least four jets with large transverse momenta, one of which is identified as originating from the fragmentation of a b quark. The data correspond to an integrated luminosity of 4.6 fb^{-1} for the μ+jets channel and 4.7 fb^{-1} for the e+jets channel. No significant excess of events over standard model expectations is observed. Assuming the strong pair production of t′ quarks, t′ quark masses below 560 GeV are excluded at 95% confidence level.

1 Introduction

The standard model (SM) contains three generations of fermions [1–3]. It is natural to ask whether there could be more than three. Experimental constraints require the corresponding neutrino to be massive, heavier than half the mass of the Z boson [4], and the masses of the quarks to be greater than 358 GeV [5, 6]. The existence of a fourth generation is consistent with precision electroweak data and would increase the upper limit on the mass of the Higgs boson, derived from precision electroweak measurements, to $\sim$500 GeV [7]. Results from precision electroweak measurements imply that the mass splitting between the up-type t' quark and the down-type b' quark of a fourth generation must be smaller than the mass of the W boson [8–10]. Thus, the t' quark cannot decay to $\mathrm{W} + \mathrm{b}'$. Assuming mixing between the three known generations and the fourth generation, the dominant decay mode of the t' quark is therefore likely to be a W boson plus a b quark.

A search is presented for the strong pair production of a t' quark and its antiparticle, both decaying into a W boson and a b or $\bar{\mathrm{b}}$ quark. One of the W bosons is assumed to decay to leptons ($\mathrm{e}\nu$ or $\mu\nu$) and the other to a quark-antiquark pair. The branching fraction into final states with at least one lepton is about 15% for electrons as well as for muons. Events are selected with a single charged lepton, missing transverse momentum, and at least four jets with high transverse momenta (p_T). This signature is not limited to quarks of a chiral fourth generation. Vector-like quarks, predicted by many physics models beyond the SM [11, 12], could give rise to the same final state.

There are also SM processes that give rise to the same signature, most notably $\mathrm{t\bar{t}}$ and W+jets production. The present search concentrates on a t' quark with a mass larger than the SM top quark. A kinematic fit to the $\mathrm{t}'\bar{\mathrm{t}}' \to \mathrm{WbW\bar{b}} \to \ell\nu\mathrm{bq\bar{q}\bar{b}}$ hypothesis is performed to assign the reconstructed objects to the decay products of the t' quark pair and to estimate the t' quark mass. Two variables are used to distinguish between signal and background. The first is the variable H_T, defined as the scalar sum of the transverse momenta of the lepton and four jets, and the missing transverse momentum. The second is the t' quark mass M_{fit} obtained from the kinematic fit. The two-dimensional distribution of H_T versus M_{fit} is tested for the presence of $\mathrm{t}'\bar{\mathrm{t}}'$ production in the data.

Events with an identified electron (muon) are classified as e+jets (μ+jets) events. The analysis procedures in the two channels are kept as similar as possible with small differences mainly driven by different trigger conditions. Finally, the results from both channels are combined statistically.

2 CMS Detector and Data Samples

CMS uses a polar coordinate system, with the z axis coinciding with the axis of symmetry of the CMS detector, and oriented in the counterclockwise proton beam direction. The x axis points towards the center of the LHC ring and the y axis points up. The polar angle θ is defined with respect to the positive z axis and ϕ is the corresponding azimuthal angle. Transverse energy is defined as energy times $\sin\theta$ and pseudorapidity is defined as $\eta = -\ln[\tan(\frac{\theta}{2})]$.

The characteristic feature of the CMS detector is the superconducting solenoid, 6 m in diameter and 13 m in length, which provides an axial magnetic field of 3.8 T. Inside the solenoid are located a multi-layered silicon pixel and strip tracker covering the pseudorapidity region $|\eta| < 2.5$ to measure the trajectories of charged particles, an electromagnetic calorimeter (ECAL) covering $|\eta| < 3.0$ made of lead tungstate crystals and a preshower detector covering $1.65 < |\eta| <$

2.6 to measure electrons and photons, and a hadronic calorimeter (HCAL) made of brass and scintillators covering $|\eta| < 3.0$ to measure jets. Muons are measured with gas detectors embedded in the return yoke of the solenoid and covering $|\eta| < 2.4$ and with the inner tracking detector. The CMS detector is nearly hermetic, allowing for momentum balance measurements in the plane transverse to the beam direction. A detailed description of the CMS detector can be found elsewhere [13].

The data used in this analysis were recorded during 2011 by the CMS experiment at the Large Hadron Collider, which delivered proton-proton collisions at $\sqrt{s} = 7$ TeV. The data analyzed correspond to an integrated luminosity of 4.7 fb^{-1} for the e+jets channel and 4.6 fb^{-1} for the μ+jets channel. The e+jets data were acquired with triggers that required at least one electron candidate with thresholds in p_T between 25 and 32 GeV. When the luminosity increased, three central jets with $p_T > 30$ GeV and $|\eta| < 2.6$ were also required. The data analyzed for the μ+jets channel were acquired with triggers that required at least one muon candidate with a p_T threshold between 30 and 40 GeV. No requirements were made on jets or missing p_T in the triggers for the μ+jets events.

The following SM background processes are modeled using Monte Carlo (MC) simulations: $\mathrm{t\bar{t}}$ production, single t quark production via the tW, s-channel and t-channel processes, W+jets, Z+jets, WW, WZ, and ZZ production (diboson production is denoted as VV on figures). All of these processes, except the dominant $\mathrm{t\bar{t}}$ production, are collectively referred to as electroweak background. The simulated $\mathrm{t'\bar{t}'}$ signal events are generated for $\mathrm{t'}$ masses of 400–625 GeV in 25 GeV steps.

For single t quark production, the POWHEG [14–16] event generator is used and for all other processes, the MADEVENT/MADGRAPH [17] event generator. In both cases PYTHIA [18] simulates additional radiation, and fragments and hadronizes the quarks and gluons into jets. The generated events are processed through the CMS detector simulation based on GEANT4 [19]. Up to 20 minimum-bias events generated with PYTHIA are superimposed on the hard-scattering events to simulate multiple collisions within the same beam crossing. The MC events are weighted to reproduce the distribution of the number of vertices in the data.

In addition, multijet events that can mimic the signature of the signal events are generated using PYTHIA. Although the cross section for multijet events is large only few events remain after the selection criteria.

The MC samples for the $\mathrm{t'\bar{t}'}$ signal correspond to between 100 and 2500 fb^{-1}, the $\mathrm{t\bar{t}}$ sample to 22 fb^{-1}, and the W+jets sample to 2.5 fb^{-1}.

3 Event Reconstruction

Events are reconstructed using the particle-flow algorithm [20] that aims to reconstruct all stable particles in an event by combining information from all subdetectors: charged tracks in the tracker and energy deposits in the electromagnetic and hadronic calorimeters, as well as signals in the preshower detector and the muon system. This procedure categorizes all particles into five types: muons, electrons, photons, charged and neutral hadrons. The energy calibration is performed separately for each particle type.

Electron candidates are reconstructed from clusters of energy deposited in the electromagnetic calorimeter. The clusters are first matched to track seeds in the pixel detector. Then, the electron candidate's trajectory is reconstructed using a dedicated modeling of the electron energy loss and is fitted with a Gaussian sum filter (GSF) algorithm [21]. Finally, the particle-flow algorithm

further distinguishes electrons from charged pions using a multivariate approach [20].

Muon candidates are identified by multiple reconstruction algorithms using hits in the silicon tracker and signals in the muon system. The stand-alone muon algorithm uses only information from the muon chambers. The tracker muon algorithm starts from tracks found in the tracker and then associates them with matching signals in the muon chambers. The global muon algorithm starts from stand-alone muons and then performs a global fit to consistent hits in the tracker and the muon system.

Jets are reconstructed by the anti-k_T jet clustering algorithm [22] with the distance parameter $R = 0.5$, as implemented in FASTJET version 2.4 [23–25], from all particles found by the particle-flow algorithm. Most jet constituents are identified and reconstructed with nearly the correct energy by the particle-flow algorithm. However, small corrections of the jet energy scale as function of p_{T} and η are applied to each jet.

The vertex with the highest sum of squared p_T of all associated tracks is taken as the hard collision primary vertex.

Jets identified as originating from a b quark by the combined secondary vertex (CSV) algorithm [26] are called b-tagged. It provides optimal b-tagging performance by combining information about impact parameter significance, the secondary vertex, and jet kinematics. The variables are combined using a likelihood ratio technique to compute the b-tag discriminator. The residual differences in the performance of the b-tagging algorithm in data and MC are accounted for by data/MC scale factors. This is done by randomly removing or adding b-tags on a jet-by-jet basis, using the p_T and η dependent scale factors discussed in [26].

The missing transverse momentum in an event is defined as the magnitude of the vector sum of the transverse momenta of all objects from the particle-flow algorithm.

4 Event Selection

For this analysis, the event selection is inspired by the selection for $\mathrm{t\bar{t}}$ events in the lepton+jets channel [27]. To reduce the background from $\mathrm{t\bar{t}}$ production, higher jet p_T requirements are applied.

Charged leptons from W boson decays, originating from decays of heavy top-like objects, are expected to be isolated from nearby jets. Therefore, the relative isolation is used to check selected leptons in this respect. It is calculated as a sum of the p_T of charged hadrons, neutral hadrons and photons in a cone of $\Delta R = \sqrt{(\Delta\phi)^2 + (\Delta\eta)^2} < 0.3$ around the lepton, divided by the lepton p_T, where $\Delta\phi$ and $\Delta\eta$ are the azimuth and pseudorapidity differences with respect to the lepton direction.

Events with exactly one isolated lepton and at least four jets with $|\eta| < 2.4$ are selected. Jets that are within a cone of $\Delta R < 0.3$ of the lepton direction are not considered. At least one jet must be identified as originating from a b quark. The thresholds for the lepton p_T are driven by the trigger requirements described in Section 2. The lepton track must have an impact parameter transverse to the beam direction with respect to the primary vertex of less than 0.02 cm and less than 1 cm along the beam direction. Missing p_T in the event must be greater than 20 GeV.

The selection for the e+jets channel requires exactly one electron with $p_T > 35$ GeV and $|\eta| < 2.5$, relative electron isolation < 0.1, and at least four jets with $p_T > 120$, 90, 50, 35 GeV. The selection for the μ+jets channel requires exactly one muon with $p_T > 35$ GeV or $p_T > 42$ GeV for two running periods with different trigger conditions, $|\eta| < 2.1$, and relative muon isolation

< 0.125, and at least four jets with $p_T > 120$, 90, 30, 30 GeV. The thresholds for the two leading jet p_Ts were selected to maximize the signal-to-background ratio. The thresholds for the lepton p_T and the third and fourth jets are driven by the trigger conditions.

Table 1 lists the number of events observed and those expected for the various background sources after selection. The cross section for $t\bar{t}$ production is taken from Ref. [28]. All other cross sections are computed with Monte Carlo for FeMtobarn processes (MCFM) [29]. The expected number of background events are calculated from the cross section and integrated luminosities given in the table. In the case of the e+jets channel, the background from WW,WZ, and ZZ production are found to be negligible. The contribution of multijet backgrounds is estimated by a data driven method to be twice as big than predicted by the simulation. The fraction of $t\bar{t}$ events retained by our selection is 0.7% for the μ+jets channel and 0.5% for the e+jets channel.

Table 2 shows the cross sections for the signal process for various t′ quark masses, along with the efficiency of the event selections in the e+jets and μ+jets channels. The efficiencies include the branching fraction of the t′ quark decay into the corresponding channel. The $t'\bar{t}'$ production cross sections are computed using HATHOR [30].

Table 1: Background cross sections, observed data, and expected number of background events for the e+jets and μ+jets samples. The uncertainties quoted are the statistical uncertainties from the MC simulations.

		e+jets events	μ+jets events
$\mathcal{L}$		4683 pb^{-1}	4601 pb^{-1}
data		4734	6448
background process	cross section		
$t\bar{t}$	165.8 pb	4000 ± 33	5536 ± 45
single t	33 pb	196 ± 3	316 ± 5
W+jets	30 μb	434 ± 13	709 ± 48
Z+jets	2.9 μb	46 ± 5	51 ± 6
WW,WZ,ZZ	67 pb	$-$	14 ± 1
multijets		73 ± 3	5 ± 5
total background		4749 ± 36	6631 ± 67

5 Mass Reconstruction

The largest background for the $t'\bar{t}'$ signal is from $t\bar{t}$ production. Both processes produce the same final states, but the t and t′ quarks have different masses, and therefore the decay kinematics can be used to discriminate between the two processes statistically. The t′ mass reconstruction is described below.

There are two steps in the t′ mass reconstruction: the assignment of reconstructed objects to the quarks, and the kinematic fit to improve the resolution of the reconstructed mass of the t′ quark candidates. Assuming the production of a $t'\bar{t}'$ pair, with the decay chain $t'\bar{t}' \to WbW\bar{b}$, $W \to \ell\nu$ and $W \to q\bar{q}$, the momenta resulting from the fit of the particles in the final state must satisfy the following three constraints with M_{fit} a free parameter that is optimized in the fit:

Table 2: Theoretical cross sections and selection efficiencies for the $t'\bar{t}'$ signal with different t' masses in the e+jets and μ+jets channels. The efficiencies include the branching fraction of about 15% for the e+jets or the μ+jets channel.

$M_{t'}$ (GeV)	cross section (pb) [30]	e+jets eff. (%)	μ+jets eff. (%)
400	1.41	4.3 ± 0.1	5.4 ± 0.1
425	0.96	4.4 ± 0.1	5.6 ± 0.1
450	0.66	4.7 ± 0.1	6.0 ± 0.1
475	0.46	4.7 ± 0.1	6.1 ± 0.1
500	0.33	4.8 ± 0.1	6.2 ± 0.1
525	0.24	4.7 ± 0.1	6.4 ± 0.1
550	0.17	4.9 ± 0.1	6.5 ± 0.1
575	0.13	4.7 ± 0.1	6.6 ± 0.1
600	0.092	4.7 ± 0.1	6.6 ± 0.1
625	0.069	4.8 ± 0.1	6.5 ± 0.1

$$m(\ell\nu) = M_W, \tag{1}$$
$$m(q\bar{q}) = M_W, \tag{2}$$
$$m(\ell\nu b) = m(q\bar{q}b) = M_{fit}. \tag{3}$$

The reconstructed objects in the event are the charged lepton, the missing transverse momentum vector, and four or more jets. The momentum of the charged lepton is measured. For the neutrino only the transverse momentum is measured by the missing transverse momentum in the event. The longitudinal component of the neutrino momentum cannot be measured, but its value can be determined from the kinematic constraints with a two-fold ambiguity. The four quarks in the final state manifest themselves as jets and their momenta can be measured. Thus, all but one of the momentum components of the final state are measured. With one unknown and three constraints, a kinematic fit is performed by minimizing the χ^2 computed from the difference between the measured momenta of all final-state particles and their fitted values, divided by the measurement uncertainty, satisfying the kinematic constraints listed above.

A study to evaluate the performance of the mass reconstruction procedure was carried out. It was shown that using up to five leading jets, when available, results in a higher percentage of correct assignments of reconstructed jets to generated quarks and a better separation between the $t'\bar{t}'$ quark signal and the $t\bar{t}$ background. Thus, in events with exactly four jets, all permutations of jet-quark assignments are considered, subject to the condition that at least one b-tagged jet must be assigned to a b quark. In events with more than four jets, the five jets that have the highest p_T are used. All combinations of four jets are considered that contain at least one jet with a b tag, and for each combination all permutations are considered, subject to the condition that at least one b-tagged jet must be assigned to a b quark. In each event, the kinematic fit is carried out for every allowed jet-quark assignment. The jet-quark assignment with the smallest value of χ^2 is chosen to reconstruct the event and the value of M_{fit} for this assignment is used as the estimator for the t' quark mass. In order to maintain maximum efficiency for the $t'\bar{t}'$ signal, no selection is applied on the value of χ^2.

Figures 1 and 2 show the M_{fit} and H_T distributions for the e+jets and μ+jets channels. The $t\bar{t}$ events that pass the selection criteria either have high-p_T t and $\bar{t}$ quarks that produce high-

momentum jets in their decay or they have high-p_T jets from initial-state radiation. The former class of events is responsible for the relatively narrow peak in the M_{fit} distribution at the t quark mass. The M_{fit} distribution of the latter class of events is broad and typically populates the region above the t-quark mass, leading to the observed high-mass tail in the M_{fit} distribution.

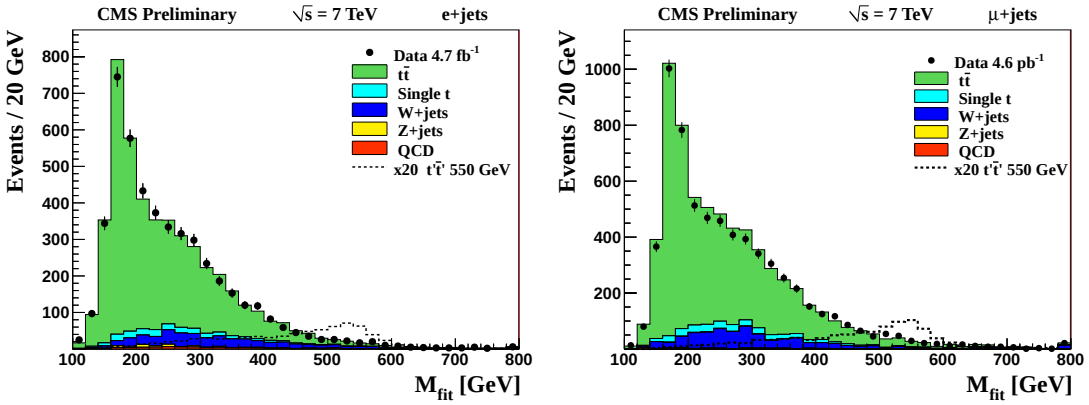

Figure 1: Distribution of M_{fit} observed (points) and simulated for backgrounds (shaded histograms) and for the t′ signal (dashed histogram) with $M_{t'} = 550$ GeV) in the e+jets (left) and μ+jets (right) channels. The signal distribution is multiplied by a factor 20 for clarity.

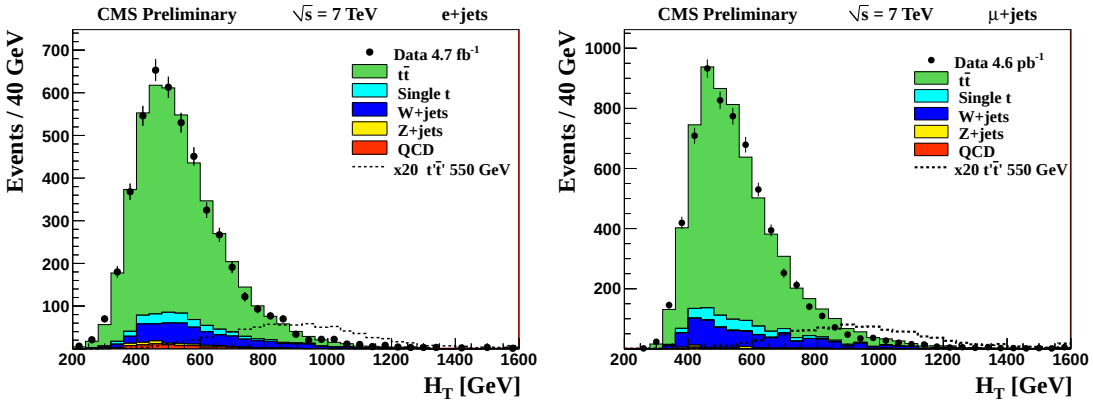

Figure 2: Distribution of H_T observed (points) and simulated for backgrounds (shaded histograms) and for the t′ signal (dashed histogram) with $M_{t'} = 550$ GeV) in the e+jets (left) and μ+jets (right) channels. The signal distribution is multiplied by a factor 20 for clarity.

6 Limit Computation

The distributions of M_{fit} and H_T of the selected events are shown in Fig. 1 and 2 for the e+jets and μ+jets channels. The corresponding two-dimensional distributions of H_T vs. M_{fit} are used to search for a $t'\bar{t}'$ signal in the data. The input distributions are shown in Fig. 3 and 4.

The SM background has two main components. The largest contribution is from $t\bar{t}$ production. Other electroweak processes (W+jets, Z+jets, single-t, and diboson production) also contribute to the final sample, although this contribution is suppressed by requiring at least one b-tagged jet in the event. A third component arises from multijet production for which the number of

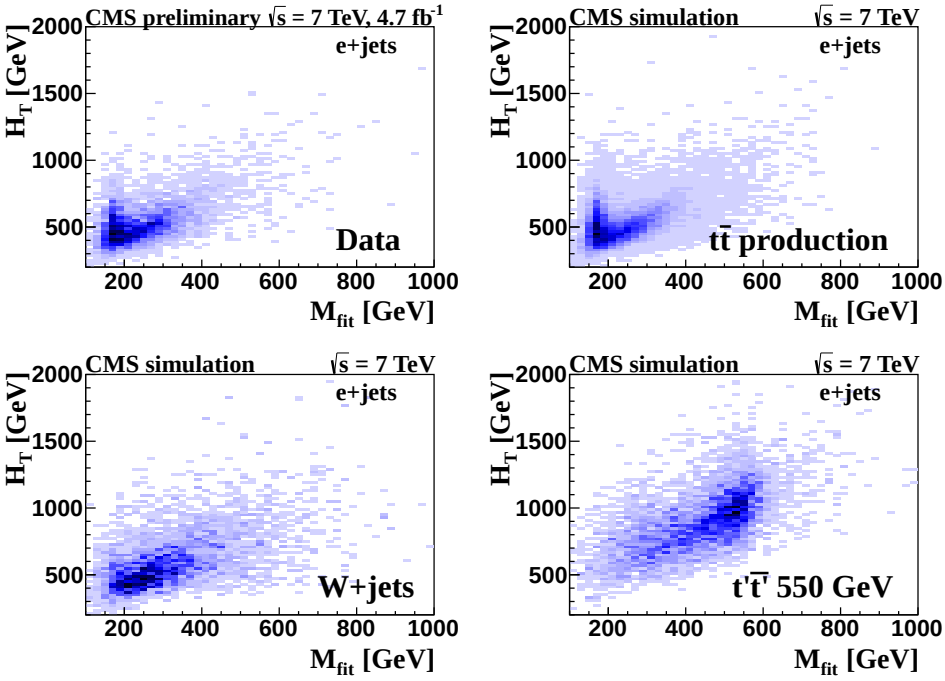

Figure 3: Histograms of H_T versus M_{fit} for the e+jets channel from (a) data, and simulations of (b) $t\bar{t}$ production, (c) W+jets background, and (d) $t'\bar{t}'$ production for $M_{t'} = 550$ GeV.

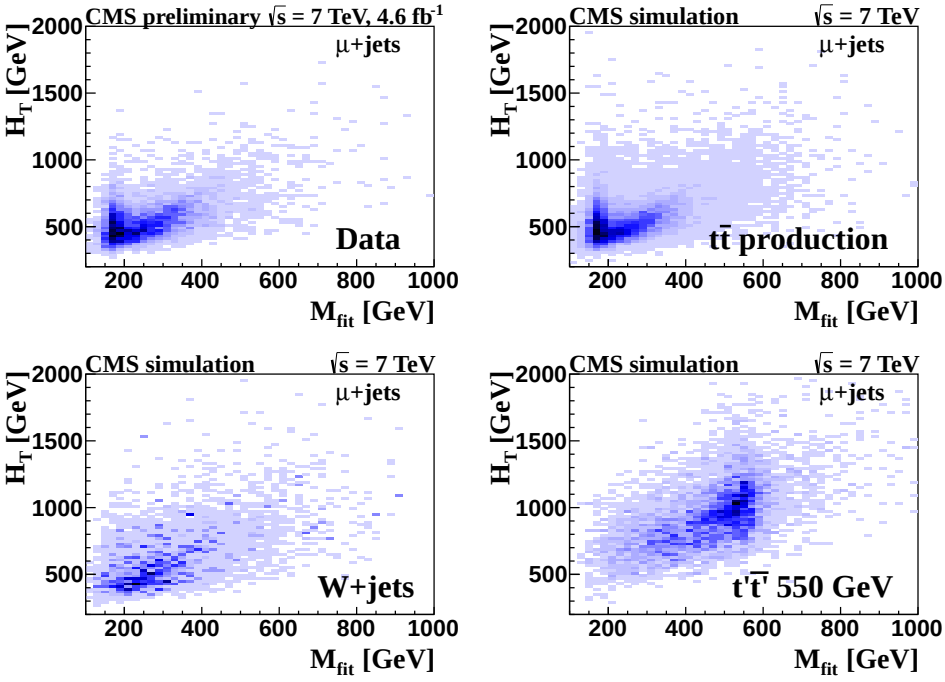

Figure 4: Histograms of H_T versus M_{fit} for the μ+jets channel from (a) data, and simulations of (b) $t\bar{t}$ production, (c) W+jets background, and (d) $t'\bar{t}'$ production for $M_{t'} = 550$ GeV.

events is small. They are added to the electroweak backgrounds according to their expected yield.

The computation of the $t'\bar{t}'$ cross section limit is performed using templates produced from data and MC simulation. The number of generated MC events is not sufficient to populate all the bins of the H_T vs M_{fit} histograms adequately. Bins in the background or signal templates that remain empty because of limited MC sample size, even though they have a small but finite probability to be occupied, could lead to incorrect statistical inferences.

Therefore, the following algorithm is employed to combine bins with inadequate statistics. First all background templates are added to obtain the expected background event yield in each bin. Then the projections of the signal and the background templates onto the H_T and M_{fit} axes are fitted with an analytic function. Bins in both signal and background templates are sorted in decreasing order of the signal/background ratio, computed as the product of the fits to the two projections, evaluated at the H_T and M_{fit} values that correspond to the bin center. Sorting bins by signal/background ratio before combining them minimizes the loss of sensitivity from the rebinning procedure. The expected signal/background ratio is not determined directly from the number of MC events in each bin, but from analytical fits to the projections of the templates onto the H_T and M_{fit} axes. In this way possible biases in the signal/background ordering due to statistical fluctuations in the signal and background templates are avoided. Finally, adjacent bins in the ordered templates are merged until the fractional statistical uncertainty in the event yield in the combined bin is below 20% for both signal and background templates. Figure 5 shows the maps of the merged bins obtained for the 550 GeV t' quark mass hypothesis. Figure 6 shows the observed number of events in each bin compared to the signal and background expectations.

The computation for the $t'\bar{t}'$ cross section limit uses the CLs method [31, 32]. The following likelihood ratio is used as test statistic:

$$t(x|\sigma) = \begin{cases} L(x|\sigma, \hat{\alpha}_\sigma)/L(x|\hat{\sigma}, \hat{\alpha}) & \text{if } \sigma > \hat{\sigma} \\ 1 & \text{if } \sigma \leq \hat{\sigma}. \end{cases} \tag{4}$$

Here, $L(x|\sigma, \alpha)$ is the likelihood of the data having the value x for the parameter of interest, the $t'\bar{t}'$ signal cross section σ, and the nuisance parameters α. The nuisance parameters parametrize effects that give rise to systematic uncertainties in the templates. They are discussed in the following Section. The likelihood reaches its maximum when $\sigma = \hat{\sigma}$ and $\alpha = \hat{\alpha}$. The symbol $\hat{\alpha}_\sigma$ refers to the values of the nuisance parameters α that maximize the conditional likelihood at a given value of σ.

Using the asymptotic approximation for the test statistic described in [33], the probability to observe a value for the likelihood ratio L that is larger than the observed value L_{obs} is determined. For the pseudo-experiments generated with background only, this probability is denoted by CL_b. For pseudo-experiments with a signal cross section σ, this probability is denoted by $CL_{s+b}(\sigma)$, which is a function of σ. The 95% confidence level (CL) upper limit for the $t'\bar{t}'$ signal cross section is the value of σ for which

$$CL_s = \frac{CL_{s+b}}{CL_b} = 0.05. \tag{5}$$

The combination of the two channels is performed by simultaneously fitting the histograms from both channels and then applying the CL_s method described above.

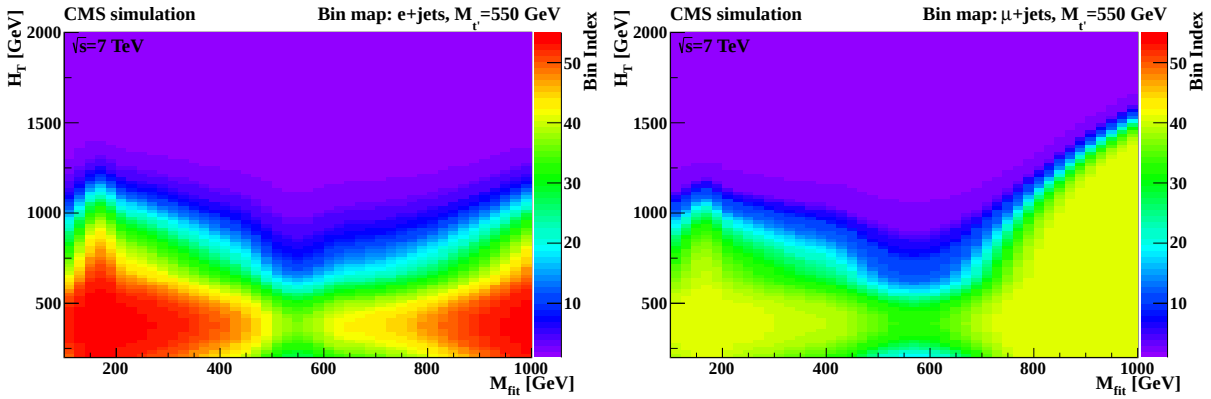

Figure 5: Map of the merged bins for the 550 GeV t′ quark mass hypothesis for the e+jets channel (left) and the μ+jets channel (right). The color represents the bin index. Low index values correspond to high signal-to-background ratios.

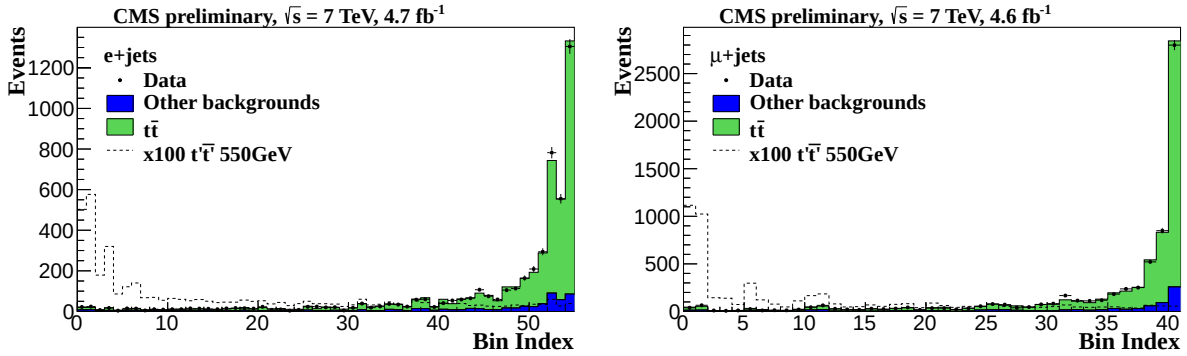

Figure 6: Histograms of templates after bin-merging for the e+jets channel (left) and μ+jets channel (right) for the 550 GeV t′ mass hypothesis.

7 Systematic Uncertainties

Systematic uncertainties influence the signal and background predictions of the discriminating distribution M_{fit} vs. H_T, used to test whether the observed events are consistent with the signal-plus-background or the background-only hypothesis. Below, all sources of systematic uncertainties are described that have been considered. They can be divided into two types: uncertainties that only impact the normalization of the H_T vs. M_{fit} distributions (normalization uncertainties), and uncertainties that also affect the shape of the distributions (shape uncertainties).

7.1 Normalization Uncertainties

The normalization uncertainties include the total $t\bar{t}$ cross section, electroweak and multijet background normalization, integrated luminosity, lepton efficiencies and data to MC scale factors.

The cross section for $t\bar{t}$ production has been measured by CMS to be 165.8 ± 13.3 pb [28]. As the luminosity uncertainty is the same for this analysis and the $t\bar{t}$ cross section measurement, only the additional uncertainty of 6.6% is taken into account in the limit calculation.

The electroweak and multijet backgrounds are constrained to the yields predicted by the cross

sections from MCFM. A 50% uncertainty is assigned to the sum of all backgrounds. Thus, its absolute normalization is mainly determined from the fit to the data.

The integrated luminosity affects the normalization of the $t'\bar{t}'$ signal and the background templates in a correlated way. The integrated luminosity is known to a precision of 4.5% [34].

Trigger efficiencies and lepton identification data/MC scale factors are obtained from data-driven techniques using decays of Z bosons to dileptons. Their uncertainties are included in the selection efficiency uncertainty. They amount to 2% for the μ+jets channel and 3% for the e+jets channel.

7.2 Shape Uncertainties

The shape uncertainties are due to the jet energy scale, jet energy resolution, resolution in missing p_T, b-tagging, multiple interactions, factorization/normalization scale Q, matrix element - parton shower matching threshold [35] and initial- and final-state radiation.

The energy of all jets is corrected by the standard CMS jet energy calibration constants [36]. Since the sum of the four-momenta of the jets is 100% correlated with the measured missing p_T, the missing p_T also changes. The jet energy scale uncertainty affects the normalization and the shape of the H_T vs. M_{fit} distribution. This is accounted for by generating the H_T vs. M_{fit} distributions for values of the jet energy scaled up or down by one standard deviation of the η- and p_T-dependent uncertainties from [36]. Thus, this uncertainty is incorporated into the cross-section limit calculation by assigning a bin content uncertainty to the H_T vs. M_{fit} distribution that is derived from the H_T vs. M_{fit} histograms found from scaling up or down the jet energy.

The energy resolution of jets in the simulation is better than in the data. Therefore smearing is applied to the jet energies to increase the resolution by 10%, to match the resolution of the detector. To account for the uncertainty in this correction, two operating points are created: no additional resolution correction and 20% resolution correction. The missing p_T resolution is also simultaneously corrected for this effect.

The missing-p_T resolution has contributions already accounted for with the jet energy scale and the jet energy resolution discussed above. In addition, there are two sources of systematic uncertainty, lepton momentum resolution and unclustered energy.

The systematic uncertainties in the b-tagging efficiency is estimated by varying the b-tagging efficiency by ± 1 standard deviation taken from [26].

To evaluate the uncertainties related to the modeling of multiple interactions in the same beam crossing, the number of interactions in the data is varied by 8%.

The uncertainty in the factorization/normalization scale Q, used for the strong coupling constant $\alpha_s(Q^2)$, is estimated by using two sets of $t\bar{t}$ MC samples in which the scale Q is increased and decreased by factors of two relative to its nominal value.

The uncertainty arising from the matrix element - parton shower matching threshold is estimated using two $t\bar{t}$ MC samples, generated with matching threshold varied up and down by a factor of two from its default value.

The impact of initial- and final-state radiation is estimated using a high-statistics $t\bar{t}$ MC sample generated with POWHEG.

7.3 Uncertainties Accounted for in the Limit Calculations

The effects of the systematic uncertainties on the expected cross section limits are estimated by adding them to the calculation one at a time. The largest effects on the expected cross section limits come from the normalizations of the electroweak background and the jet energy scale calibration. The normalization of the $t\bar{t}$ background also has a significant effect on the limits. The lepton efficiency uncertainties and the other shape uncertainties all change the expected limits by very small amounts. Therefore the following uncertainties are considered in the limit calculation by assigning nuisance parameters to them: integrated luminosity, normalization of the electroweak and $t\bar{t}$ backgrounds, lepton efficiency, jet energy scale and parton-shower matching threshold. The effect of any of the other uncertainties studied is negligible when added to this list.

8 Results

Figure 7 shows the observed and expected 95% CL upper limit on the $t'\bar{t}'$ cross section for the μ+jets channel (top), the e+jets channel (middle), and the combination of both channels (bottom). The upper limit for the t' quark mass is given by the value at which the observed upper limit curve for the $t'\bar{t}'$ cross section crosses the theoretical curve. In the μ+jets channel this happens for the 95% CL observed (expected) limits for t' quark masses of 550 (550) GeV. In the e+jets channel the corresponding t' quark mass values are 485 (530) GeV. The combined observed (expected) limits from both channels are 560 (580) GeV.

9 Summary

The CMS experiment has performed a search for the production of up-type fourth-generation $t'\bar{t}'$ quark pairs, where each quark decays exclusively to Wb, and one of the W decays to leptons and the other to a quark-antiquark pair. Events are selected with an electron or a muon, significant missing transverse momentum, and at least four jets of which one is identified as a b jet. A kinematic fit assuming $t'\bar{t}'$ production is performed and for every event a candidate t' quark mass and the sum over the transverse momenta of all decay products of the $t'\bar{t}'$ system are reconstructed. No significant deviations from standard model expectations are found in this two-dimensional distribution and upper limits are set on the production cross section of such t' quarks as a function of their mass. By comparing with the predicted cross section for $t'\bar{t}'$ production, the strong pair production of t' quarks can be excluded at 95% CL for masses below 560 GeV under the model assumptions used in this analysis.

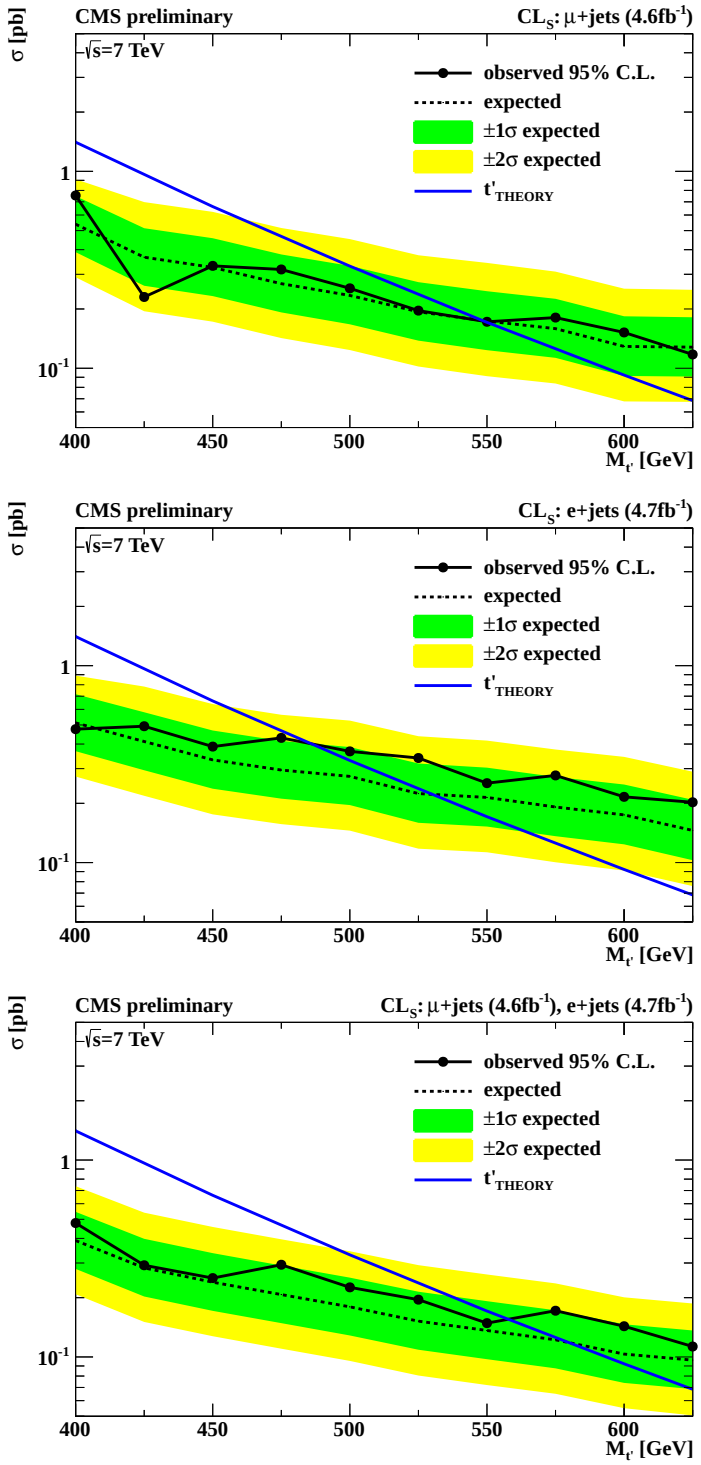

Figure 7: The observed (solid line with points) and the expected (dotted line) 95% CL upper limits on the $t'\bar{t}'$ production cross section as a function of the t' quark mass for μ+jets (top), e+jets (middle) and combined (bottom) analyses. The ± 1 and ± 2 standard deviation ranges on the expected limit are shown by the bands. The theoretical cross section is shown by the continuous line without points.

References

[1] S. L. Glashow, "Partial Symmetries of Weak Interactions", *Nucl. Phys.* **22** (1961) 579–588. doi:10.1016/0029-5582(61)90469-2.

[2] S. Weinberg, "A Model of Leptons", *Phys. Rev. Lett.* **19** (Nov, 1967) 1264–1266. doi:10.1103/PhysRevLett.19.1264.

[3] A. Salam, "Weak and Electromagnetic Interactions", in *Elementary particle theory*, N. Svartholm, ed., pp. 367–377. Almquist & Wiksell.

[4] ALEPH Collaboration, DELPHI Collaboration, L3 Collaboration, OPAL Collaboration, SLD Collaboration, LEP Electroweak Working Group and SLD Electroweak and Heavy Flavour Groups, "Precision electroweak measurements on the Z resonance", *Physics Reports* **427** (2006) 257.

[5] D0 Collaboration, "Search for a fourth generation t' quark in $p\bar{p}$ collisions at $\sqrt{s} = 1.96$ TeV", *Phys. Rev. Lett.* **107** (2011) 082001, arXiv:hep-ex/1104.4522.

[6] CDF Collaboration, "Search for Heavy Top $t' \to Wq$ in Lepton Plus Jets Events in $\int \mathcal{L}dt = 5.6$ fb^{-1}", *Phys. Rev. Lett.* **107** (2011) 261801, arXiv:hep-ex/1107.3875.

[7] H.-J. He, N. Polonsky, and S.-F. Su, "Extra families, Higgs spectrum and oblique corrections", *Phys. Rev.* **D64** (2001) 053004, arXiv:hep-ph/0102144.

[8] G. D. Kribs, T. Plehn, M. Spannowsky et al., "Four generations and Higgs physics", *Phys. Rev.* **D76** (2007) 075016, arXiv:0706.3718.

[9] A. Soni, A. K. Alok, A. Giri et al., "SM with four generations: Selected implications for rare B and K decays", *Phys. Rev.* **D82** (2010) 033009, arXiv:1002.0595.

[10] O. Eberhardt, A. Lenz, and J. Rohrwild, "Less space for a new family of fermions", *Phys. Rev.* **D82** (2010) 095006, arXiv:1005.3505.

[11] D. Choudhury, T. Tait and C. Wagner, "Beautiful Mirrors and Precision Electroweak Data", *Phys. Rev. D* **65** (2002) 053002, arXiv:hep-ph/0109097.

[12] M. Schmaltz, "Physics beyond the standard model (theory): Introducing the little Higgs", *Nucl. Phys. Proc. Suppl.* **117** (2003) 40–49, arXiv:hep-ph/0210415.

[13] CMS Collaboration, "The CMS experiment at the CERN LHC", *JINST* **3** (2008) S08004. doi:10.1088/1748-0221/3/08/S08004.

[14] P. Nason, "A New method for combining NLO QCD with shower Monte Carlo algorithms", *JHEP* **0411** (2004) 040.

[15] S. Frixione, P. Nason, and C. Oleari, "Matching NLO QCD computations with Parton Shower simulations: the POWHEG method", *JHEP* **0711** (2007) 070.

[16] S. Alioli, P. Nason, C. Oleari, and E. Re, "A general framework for implementing NLO calculations in shower Monte Carlo programs: the POWHEG BOX", *JHEP* **1006** (2010) 043.

[17] J. Alwall, P. Demin, S. de Visscher et al., "MadGraph/MadEvent v4: The New Web Generation", *JHEP* **0709** (2007) 028, arXiv:0706.2334.

[18] T. Sjöstrand, S. Mrenna, and P. Z. Skands, "PYTHIA 6.4 Physics and Manual", *JHEP* **05** (2006) 026, arXiv:hep-ph/0603175. doi:10.1088/1126-6708/2006/05/026.

[19] GEANT4 Collaboration, "GEANT4: A simulation toolkit", *Nucl. Instrum. Meth.* **A506** (2003) 250–303. doi:10.1016/S0168-9002(03)01368-8.

[20] CMS Collaboration, "Particle-Flow Event Reconstruction in CMS and Performance for Jets, Taus, and MET", *CMS PAS PFT-09-001* (2009).

[21] W. Adam, R. Fruhwirth, A. Strandlie, T. Todorov, "Reconstructions of Electrons with the Gaussian-Sum Filter in the CMS Tracker at the LHC", *J. Phys. G: Nucl. Part. Phys.* **31** (2005) N9–N20.

[22] M. Cacciari, G. P. Salam, and G. Soyez, "The Anti-k(t) jet clustering algorithm", *JHEP* **0804** (2008) 063, arXiv:0802.1189.

[23] M. Cacciari and G. P. Salam, "Dispelling the N^3 myth for the k_t jet-finder", *Phys.Lett.* **B641** (2006) 57–61, arXiv:hep-ph/0512210.

[24] M. Cacciari, G. P. Salam, and G. Soyez, "The Catchment Area of Jets", *JHEP* **0804** (2008) 005, arXiv:0802.1188.

[25] M. Cacciari and G. P. Salam, "Pileup subtraction using jet areas", *Phys. Lett.* **B659** (2008) 119–126, arXiv:0707.1378.

[26] CMS Collaboration, "Measurement of the b-tagging efficiency using $t\bar{t}$ events", *CMS Physics Analysis Summary* **CMS-PAS-BTV-11-003** (2011).

[27] CMS Collaboration, "Measurement of the tt Pair Production Cross Section at $\sqrt{s}$ = 7 TeV using b-quark Jet Identification Techniques in Lepton + Jet Events", *CMS Physics Analysis Summary* **CMS-PAS-TOP-11-003** (2011).

[28] CMS Collaboration, "Combination of top quark pair production cross section measurements", *CMS Physics Analysis Summary* **CMS-PAS-TOP-11-024** (2011).

[29] J. M. Campbell and R. Ellis, "Next-to-leading order corrections to $W+$ 2 jet and $Z+$ 2 jet production at hadron colliders", *Phys. Rev.* **D65** (2002) 113007, arXiv:hep-ph/0202176. doi:10.1103/PhysRevD.65.113007.

[30] M. Aliev et al., "– HATHOR – HAdronic Top and Heavy quarks crOss section calculatoR", *Comput. Phys. Commun.* **182** (2011) 1034–1046, arXiv:1007.1327.

[31] T. Junk, "Confidence level computation for combining searches with small statistics", *Nucl. Instrum. Meth.* **A434** (1999) 435–443, arXiv:hep-ex/9902006.

[32] A. L. Read, "Presentation of search results: The CL(s) technique", *J. Phys. G* **G28** (2002) 2693–2704. doi:10.1088/0954-3899/28/10/313.

[33] G. Cowan, K. Cranmer, E. Gross et al., "Asymptotic formulae for likelihood-based tests of new physics", *Eur.Phys.J.* **C71** (2011) 1554. doi:10.1140/epjc/s10052-011-1554-0.

[34] CMS Collaboration, "Absolute Luminosity Normalization", *CMS Detector Performance Summary* **CMS-DP-2011-003** (2011).

[35] S. Mrenna and P. Richardson, "Matching matrix elements and parton showers with HERWIG and PYTHIA", *JHEP* **0405** (2004) 040, arXiv:0312.274.

[36] CMS Collaboration, "Determination of jet energy calibration and transverse momentum resolution in CMS", *JINST* **6** (2011) P11002, arXiv:1107.4277.